# p-Type $MoS_2$ and n-Type ZnO Diode and Its Performance Enhancement by the Piezophototronic Effect

*Fei Xue, Libo Chen, Jian Chen, Jingbin Liu, Longfei Wang, Mengxiao Chen, Yaokun Pang, Xiaonian Yang, Guoyun Gao, Junyi Zhai,* and Zhong Lin Wang**

2D molybdenum disulfide ($MoS_2$) is emerging as an excellent layered material with superior electrical, optical, and piezoelectrical properties.[1–10] The commonly found semiconducting $MoS_2$ presents a hexagonal crystal structure, constructed by a layer of molybdenum atoms sandwiched between two layers of sulfide atoms. The bulk $MoS_2$, belonging to $D_{6h}$ crystal structure space group, possesses an indirect bandgap of ≈1.2 eV while the monolayer $MoS_2$, belonging to $D_{3h}$ space group, owns a direct bandgap of ≈1.85 eV.[11,12] A series of these 2D $MoS_2$ functional devices have been demonstrated, including field-effect transistors (FETs),[1,2] photodetectors,[4,5] touch sensors,[13,14] and chemical sensors.[15,16] Interestingly, the odd-layer $MoS_2$ flake is currently confirmed to possess a strong piezoelectric coefficient along its $d_{11}$ or $e_{11}$ direction[7–10] and demonstrated as nanogenerators for harvesting micromechanical energy.[8] Additionally, vertically or laterally stacked heterostructures based on the atomically thin $MoS_2$, such as $MoS_2/WSe_2$,[17,18] $MoS_2$/graphene[19,20] and $MoS_2/WS_2$,[21,22] have also been extensively studied. However, in those heterostructure configurations, the pristine $MoS_2$ crystal plays a role of an n-type semiconductor. Up to now, a few works are reported to utilize electrostatic field,[23] chemical element,[24] and plasma[25] to change the carrier type of $MoS_2$ and demonstrate a p-type semiconductor.

The traditional "3D" semiconductors-based p–n junctions, including Si and GaN, are the most fundamental building blocks for modern electronic and optoelectronic devices. To explore new observations and functionality, some efforts have been made to integrate the 2D layered $MoS_2$ on those conventional semiconductors to achieve functional p–n heterojunctions, such as light emission from n-$MoS_2$ and p-GaN,[26] photoresponse from n-$MoS_2$ and p-Si.[27] Zinc oxide (ZnO) is a semiconductor with a crystal structure of hexagonal wurtzite and a direct wide-bandgap of 3.4 eV. In the past decade, numerous works have reported ZnO-based smart devices with external strain sensitively perceived.[28–33] Here, we report an $MoS_2$ flake and ZnO film based vertically heterojunction p–n diode, in which the p-type $MoS_2$ is effectively doped via a plasma-assisted method and the n-type ZnO grown by pulsed laser deposition (PLD). The $MoS_2$ and ZnO p–n diode shows ambipolar carrier transport, high forward-to-reverse current ratio ($3.4 \times 10^4$), and large reverse saturation current range (1.5 V). Under the optical irradiation of 365 nm, this p–n diode exhibits strong photoresponse with an external quantum efficiency (EQE) of 52.7% and response time of 66 ms. In additional, as the externally applied pressure on the junction increases to 23 MPa, the photocurrent of this device can be enhanced for more than four times by the piezophototronic effect. This heterojunction p–n diode provides a technical route for achieving smart tactile and high-performance electronic and optoelectronic devices.

Multilayer $MoS_2$ flakes were exfoliated from the bulk material and then transferred to a highly doped n-type Si with 300 nm thickness $SiO_2$. The $MoS_2$ flakes with about 20–50 nm thickness were preliminarily selected by optical microscopy and atomic force microscopy, which would be easily realized atomically doped samples after the follow-up process. The inductively coupled plasma (ICP) with an $SF_6$ reactive gas was used to effectively dope the obtained $MoS_2$ samples. **Figure 1**a shows a schematic illustration of multilayers $MoS_2$ doping process. Due to the sulfide vacancies in the pristine $MoS_2$, the samples prepared by the method of mechanical exfoliation or chemical vapor deposition always present n-type,[1,2,15] in which electrons dominate the carriers transport. After $MoS_2$ is treated with $SF_6$ plasma, external fluorine (F) atoms will be introduced into the semiconductor, resulting in charge transfer between incorporated atoms (F) and $MoS_2$ layers. The F atoms have relatively strong electronegativity and will preferentially attract the excess electrons in pristine $MoS_2$ layers, giving rise to a new p-type $MoS_2$.[25] However, during the plasma-assisted doping process, multilayer $MoS_2$ will be inevitably thinned under ion bombardment and the highly doped region only restricted on the exposed surface of $MoS_2$, as indicated on the right-hand diagrams of Figure 1a.

Figure 1b presents optical images of the same $MoS_2$ flake before and after treating with $SF_6$ plasma. The exfoliated $MoS_2$ pristine sample with thickness of 30.5 nm is distinctly reduced to 3.1 nm (Figure 1b; Figure S1, Supporting Information) after disposed by the plasma. Roman spectra on the right-hand diagrams of Figure 1b show that the strong $E_{2g}$ and $A_{1g}$ peaks exist and the distance between them is 23 $cm^{-1}$, indicating that the treated $MoS_2$ is four layers with smooth surface.[13,15] To validate the p-type property, the treated $MoS_2$ flakes with different layers are used to fabricate FETs for systematically observing

F. Xue, L. Chen, J. Chen, J. Liu, L. Wang, M. Chen, Y. Pang, X. Yang, G. Gao, Prof. J. Zhai, Prof. Z. L. Wang
Beijing Institute of Nanoenergy and Nanosystems
Chinese Academy of Sciences
National Center for Nanoscience and Technology (NCNST)
Beijing 100083, P. R. China
E-mail: jyzhai@binn.cas.cn; zhong.wang@mse.gatech.edu
Prof. Z. L. Wang
School of Materials Science and Engineering
Georgia Institute of Technology
Atlanta, GA 30332, USA

DOI: 10.1002/adma.201506472


© 2016 WILEY-VCH Verlag GmbH & Co. KGaA, Weinheim

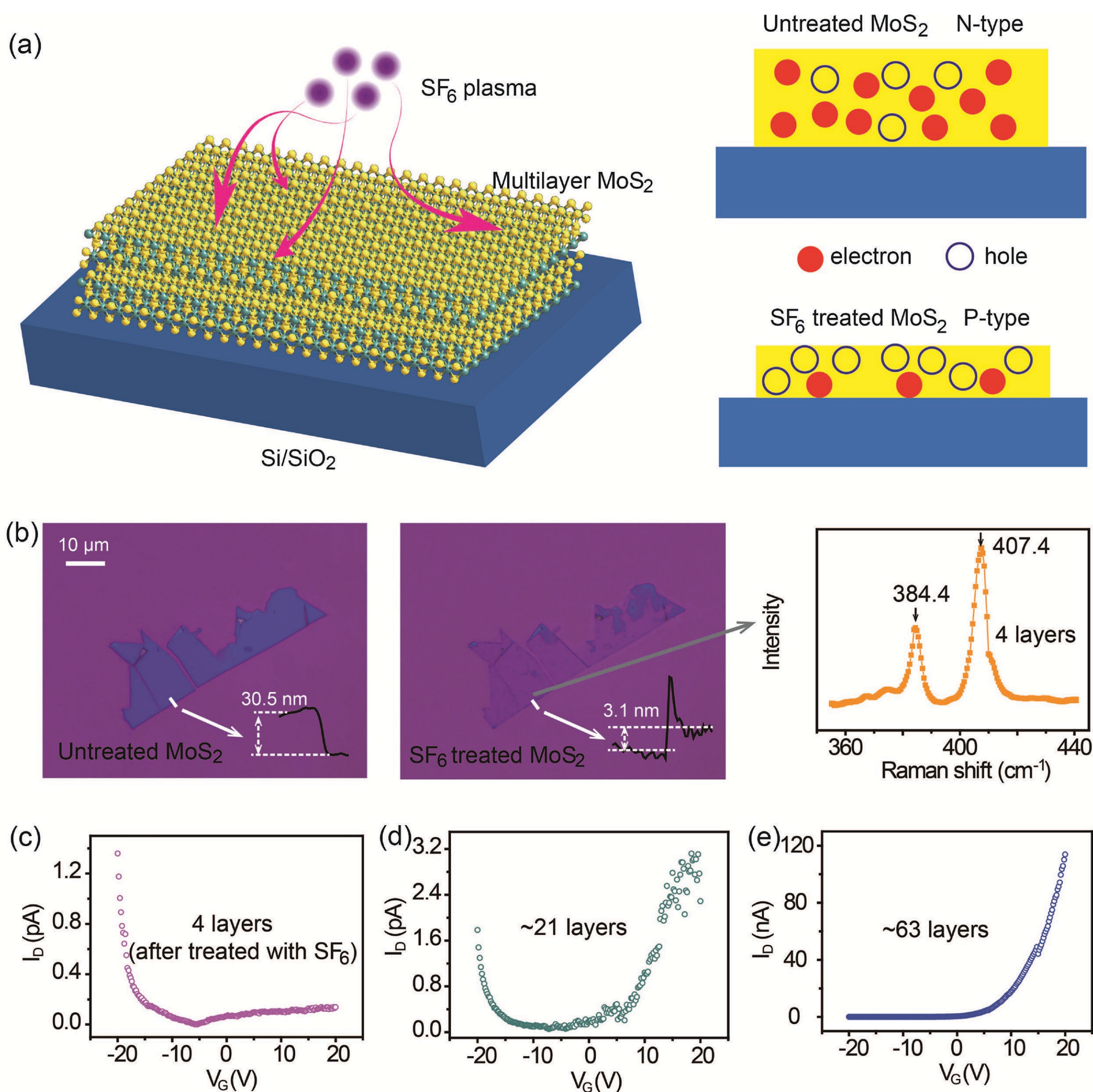


**Figure 1.** Interpretation of the doping mechanism. a) Schematic illustration of a doped multilayer $MoS_2$ sample by a plasma-assisted method. After treating with $SF_6$ plasma, the $MoS_2$ flake will be inevitably thinned and turn to a p-type semiconductor. b) False-color optical images for comparison of the untreated and treated $MoS_2$ flake. The bulk $MoS_2$ is reduced to the atomic thickness by accurately controlling the time and power of $SF_6$ plasma. c–e) $I_D$–$V_G$ transfer curves for $MoS_2$ transistors with different layers, which have been disposed by $SF_6$ plasma beforehand. All of the drain biases ($V_D$) are fixed at 2 V.

the electrical transport characteristics, as shown in Figure 1c–e. The $I_D$–$V_G$ transfer curves illustrate that with the increasing layers, the hole-dominated $MoS_2$ (p-type) FET will experience a transition to an electron-dominated (n-type). The ambipolar transport also appears in a medium thickness (≈21 layers) of $MoS_2$ sample (Figure 1d). The plasma-doped region is only limited to nanometers thickness of the $MoS_2$ surface exposed under the plasma gas while the gate bias modulate the channel conductivity at the bottom surface of $MoS_2$.[25,35] Therefore, when the whole $MoS_2$ sample is nearly completely doped and atomically thick (four layers), the decreased p-type characteristic, as the gate bias increases, will emerge, which is not observed in an ≈63 layers $MoS_2$. It is notable that the applied gate voltage depletes the $MoS_2$ conductive channel via the metal-insulator-semiconductor (MIS) structure and less carriers pass through the channel, leading to low drain-source currents (≈pA), as shown in Figure 1c,d. Those results elucidate that the plasma-assisted method is an effective way to change the pristine n-type to p-type, especially for a treated $MoS_2$ sample with atomic thickness.

Next, the $SF_6$ plasma-treated $MoS_2$ sample is used as a building block with n-type ZnO deposited by PLD to achieve a heterojunction p–n diode. **Figure 2**a shows the side view of the device structure. An insulating $Al_2O_3$ layer was deposited


© 2016 WILEY-VCH Verlag GmbH & Co. KGaA, Weinheim
Adv. Mater. 2016, DOI: 10.1002/adma.201506472

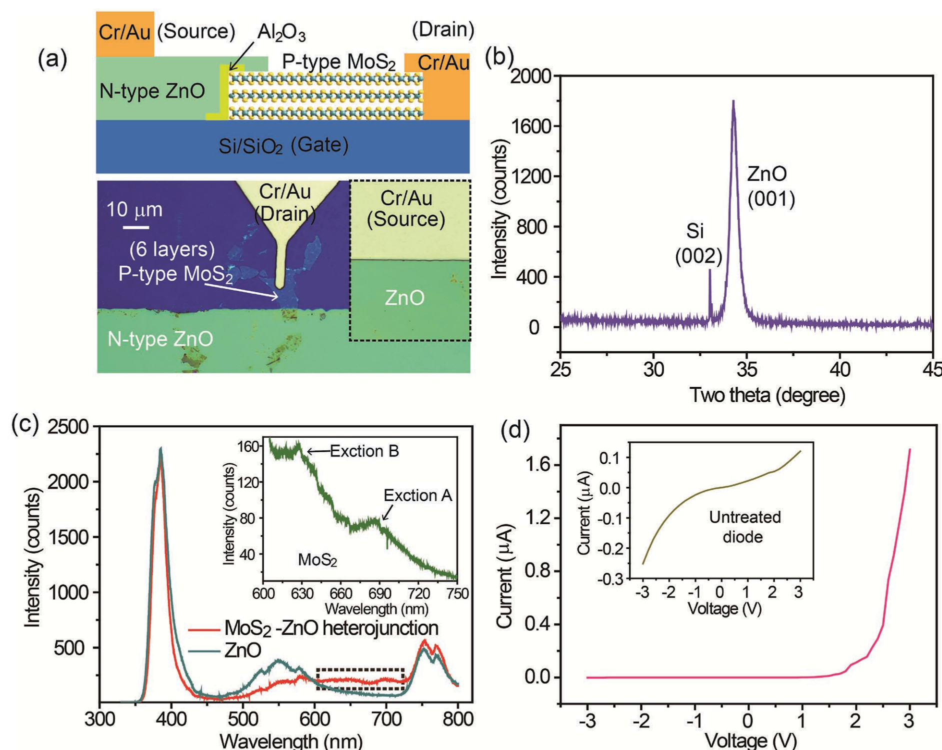


**Figure 2.** Structure of the $MoS_2$–ZnO heterojunction p–n diode and characterization of ZnO and $MoS_2$. a) Side view of the schematic structure of the p-type $MoS_2$ and n-type ZnO diode (top) and optical image of a typical device (bottom). b) XRD image showing a good *c*-axis orientation of ZnO film deposited by PLD. c) PL spectra from the $MoS_2$–ZnO heterojunction and the isolated ZnO film. Inset: PL spectra from the isolated multilayer $MoS_2$ in the junction. d) A typical rectifying curve for the $MoS_2$–ZnO heterojunction p–n diode. Inset: a $MoS_2$–ZnO heterojunction (n–n) based device without $SF_6$ plasma treatment.

on the part edge of $MoS_2$ so as to form a typically vertical p–n junction. The optical image of a typical device is shown at the bottom of Figure 2a and the chosen $MoS_2$ flake in this configuration six layers. The X-ray diffraction (XRD) image presented in Figure 2b shows that a strong (001) peak is located at 34.3°, illustrating that the deposited ZnO film has a good *c*-axis orientation.[34] The $MoS_2$ and ZnO p–n junction is also characterized by the photoluminescence (PL) spectra as shown in Figure 2c. To identify and understand the junction PL spectra, the relevant PL spectra of $MoS_2$ flake and ZnO film is also organized together for comparison. The strong peaks at 382 nm denote the ZnO intrinsic emission corresponding to bandgap, while the broad peak at 550 nm denotes the ZnO deep-level-impurities emission, and the broad peak at 755 nm denotes the ZnO shallow-level-impurity emission. The PL spectra from the $MoS_2$ flake exhibits two weak exciton peaks, which corresponds to exciton A at 687 nm and exciton B at 622 nm as shown in the inset. When two semiconducting materials (p-$MoS_2$ and n-ZnO) are vertically stacked together, the PL spectra of this hybrid structure shows that the peak at 550 nm is weakened possibly owing to the residuals on the junction and a broad peak between 600 and 720 nm appears due to the existence of two exciton peaks in $MoS_2$ as labeled in dashed line and Figure S2 (Supporting Information). Figure 2d displays a typical current–voltage output characteristic of the p–n diode, showing a good rectification behavior. The inset presents a contrastive output curve of an n-type $MoS_2$ (pristine crystal) and n-type ZnO heterojunction, demonstrating that the $SF_6$ plasma plays a critical role in changing carrier type of pristine $MoS_2$ to p-type.

**Figure 3** shows the gate bias tunable electrical characteristics of the p-type $MoS_2$ and n-type ZnO diode. With the gate bias increased from −1 to 0.5 V, the positive drain current substantially decreases as shown in Figure 3a. Correspondingly, the turn-on voltage presented in the inset varies from 0.9 to 2.6 V. Figure 3b displays the transfer characteristic of the p–n diode at a drain bias of 0.5 V, showing an ambipolar property. To clearly observe and analyze the electrical transport under different gate bias, semilogarithmic plots of the drain current ($I_D$) as a function of drain voltage ($V_D$) are displayed in detail in Figure 3c and Figure S3 (Supporting Information). Those curves consist of four regions: (1) reverse tunneling region, (2) reverse saturation region, (3) ideal linear diode region, and (4) series-resistance-dominated region. At high reverse drain bias, the energy difference between the Fermi-levels of $MoS_2$ and ZnO will be markedly enlarged, producing a much thin potential barrier.[35] The carriers in the p–n junction can easily tunnel through this barrier and the corresponding reverse current will increase with reverse drain bias increased as shown in the region "1" of Figure 3c. Although the gate bias varies, the reverse saturation current keeps invariably stable at about $3 \times 10^{-11}$ A under 1.5 V drain bias changing range (region "2"), which is almost close to the ideal reverse current model of silicon-based p–n diodes.[35] The nearly linear relationship between $I_D$ and $V_D$ in the region "3" follows the ideal Shockley diode model, from


© 2016 WILEY-VCH Verlag GmbH & Co. KGaA, Weinheim

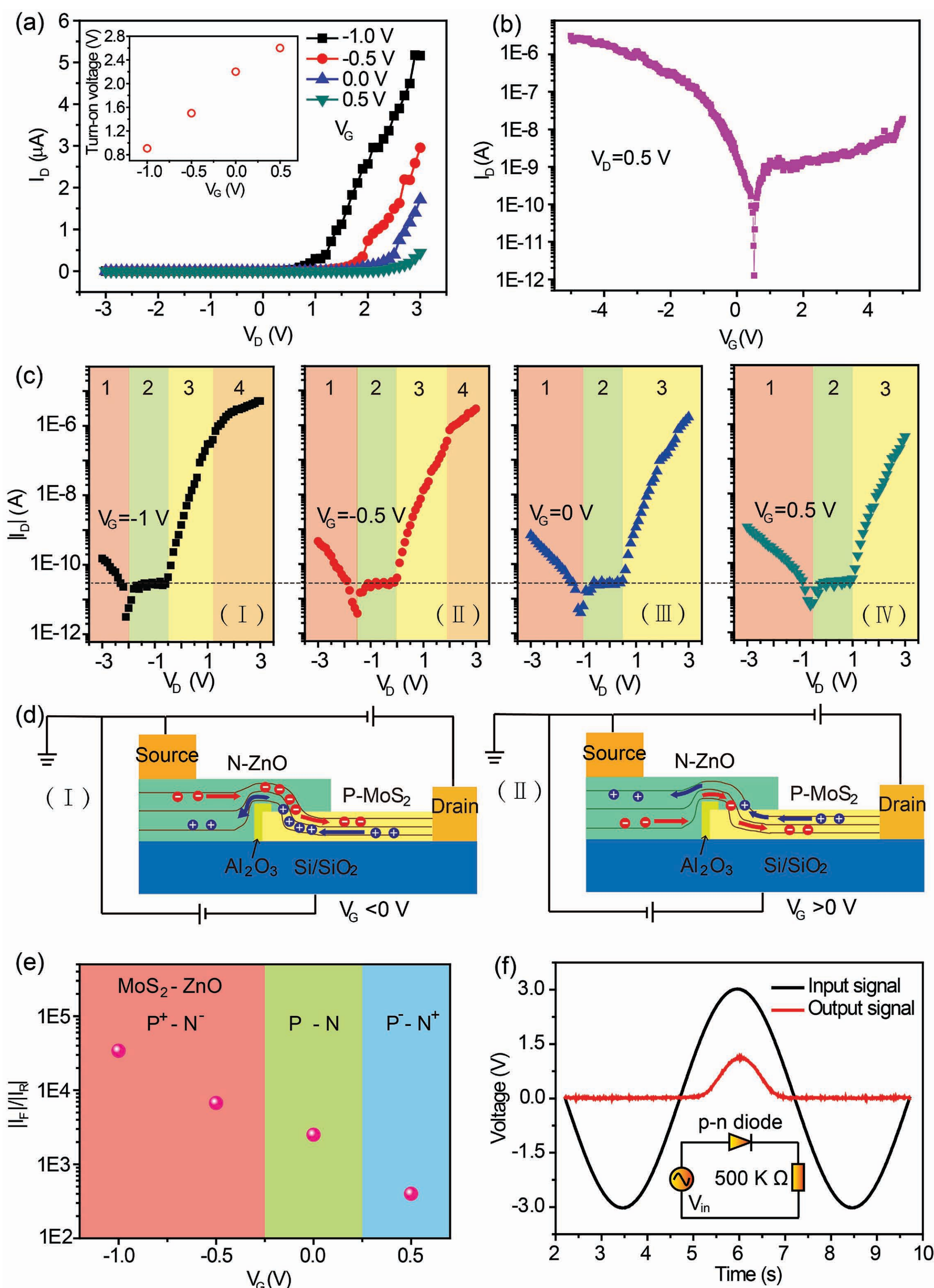


**Figure 3.** Electric properties of the $MoS_2$–ZnO heterojunction p–n diode. a) Gate tunable output characteristics showing the decreasing forward current with the increasing gate voltage. Inset: the change in turn-on voltage with different gate voltages. b) Transfer characteristics of the p–n heterojunction, indicating an ambipolar property. c) Semilogarithmic plots of the $I_D$ as a function of $V_D$ under different gate voltages, which is derived from (a). The four labeled regions represent: (1) reverse tunneling region, (2) reverse saturation region, (3) ideal linear diode region, and (4) series resistance-dominated region. d) The cross-section views illustrating the carriers transport across the p–n junction at the negative gate bias ($V_G < 0$ V) and the positive gate bias ($V_G > 0$ V). e) The gate bias dependence of forward-to-reverse current ratio (at a heterojunction bias voltage of 3 V). At a positive gate voltage, the negative free charges will be injected into the two semiconductors via the MIS structure, resulting in a $p^-$–$n^+$ junction and a low rectification ratio. f) Demonstration of the rectifying property of the p–n diode. The gate bias is set as 0 V.


© 2016 WILEY-VCH Verlag GmbH & Co. KGaA, Weinheim
Adv. Mater. 2016,
DOI: 10.1002/adma.201506472

which the ideal factor of ≈4.3 can be derived. This relatively big ideal factor may be attributed to the carriers interface recombination[35,36] compared with the ideal diode in p-$MoSe_2$/n-$MoSe_2$ and p-$MoS_2$/n- $MoS_2$.[37,38] The series resistance in the p–n diode at high forward drain voltage will share much more potential drop than the junction and dominate the $I_D$–$V_D$ curves, especially at the gate bias of −1 and −0.5 V as shown in the region "4." When the gate bias is negative, the free holes will accumulate in the bottom surface of $MoS_2$ and ZnO. Driven by the positive forward drain bias, much more majority carriers in the two semiconductors inject into the junction area (depletion zone) as shown in Figure 3d (I). By contrast, under the negative gate bias, free electrons will accumulate and few majority carriers pass through the junction area (Figure 3d (II)). This is the reason that the increased turn-on voltage and the decreased positive forward drain current appear with the gate bias increased from negative voltage to positive voltage as shown in Figure 3a. As an important parameter to characterize the heterojunction p–n diode, the forward-to-reverse current ratio ($|I_F/I_R|$) at a heterojunction bias of 3 V with the gate bias varying is presented in Figure 3e. The rectification ratio ($|I_F/I_R|$) changes about two orders of magnitude as a function of gate voltage. When the gate bias varies from −1 to 0.5 V, electrostatic doping level of $MoS_2$ and ZnO will alter and the relevant heterojunction changes from $p^+$–$n^-$ type to $p^-$–$n^+$ type. The rectifying property of the p–n diode is demonstrated in Figure 3f. With an external 500 kΩ resistance connected to the circuit in series, the p–n diode shows a good signal selection.

The photoresponse of this heterojunction p–n diode at the gate bias of 0 V is systematically shown in **Figure 4**. Ultraviolet

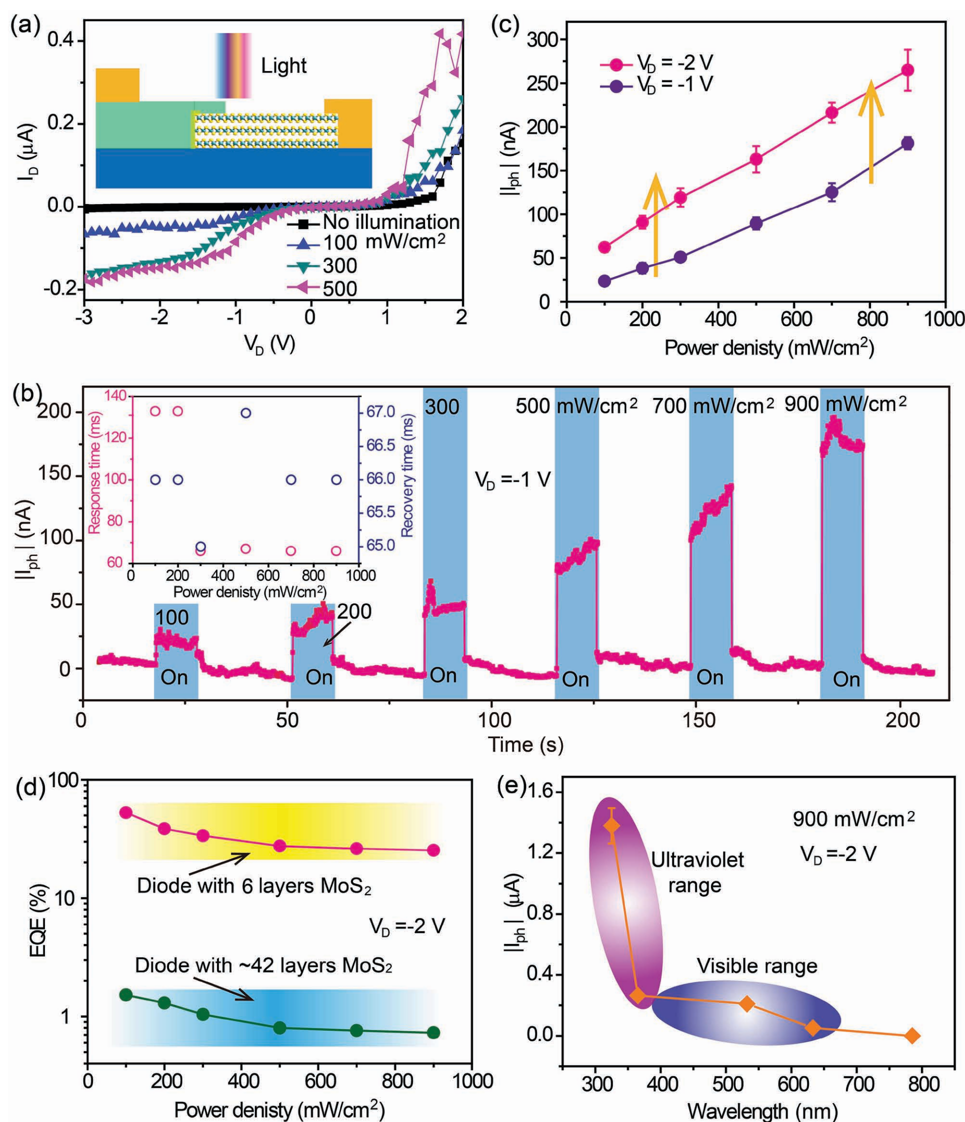


**Figure 4.** Photoresponse of the p-type $MoS_2$ and n-type ZnO diode. a) $I_D$–$V_D$ output curves under different power density of the incident light. The excitation wavelength in (a–d) is fixed at 365 nm while the gate bias in (a–e) is 0 V. b) The $I_{ph}$ response for different power intensity with an excitation light of periodic 10 s illumination. The inset presents the response times and the recovery times under different power density. c) The power density dependence of the photocurrent under different drain bias. The data at the drain voltage of −1 V is derived from (b). d) EQE as a function of incident power density with diodes possessing different thickness of $MoS_2$. e) The changeable $I_{ph}$ related to the incident light with different wavelengths.


© 2016 WILEY-VCH Verlag GmbH & Co. KGaA, Weinheim

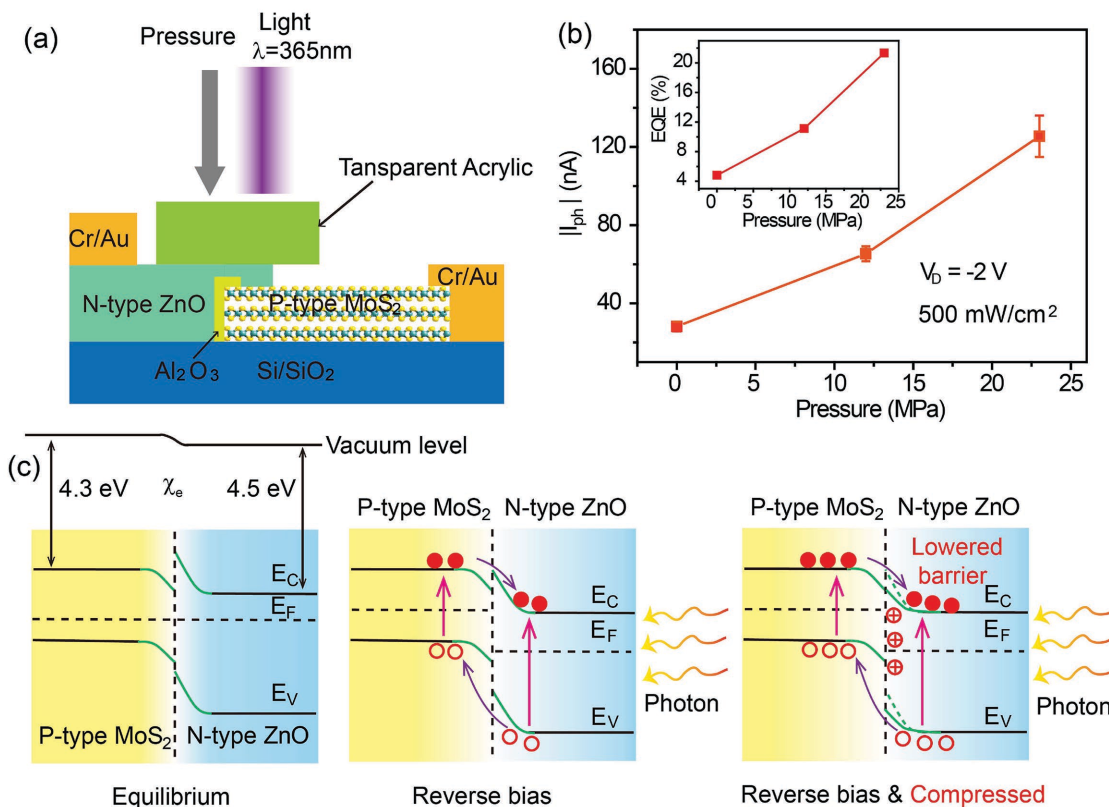


**Figure 5.** Enhanced photocurrent of the p-type $MoS_2$ and n-type ZnO photodiode by the piezophototronic effect. a) Schematic side view of the experimental set-up for testing the diode. b) Pressure dependence of the $I_{ph}$ at the drain bias of −2 V and incident power density of 500 mW $cm^{-2}$. The inset shows the increased EQE with the applied pressure increased. c) Band diagrams interpreting the photogenerated carriers and the piezophototronic effect enhanced photocurrent. The green lines in the band structure represent the relevant depletion region.

light ($\lambda$ = 365 nm) was used to excite the $MoS_2$ and ZnO heterojunction p–n diode. With the excitation power density increased, the drain current ($I_D$) is drastically increased both in the forward bias range and the negative bias range (Figure 4a). To legibly interpret the photoresponse of the diode, the ultraviolet light was controlled to periodically illuminate the device at an excitation time of 10 s and the corresponding photocurrent ($I_{ph} = I_{excited} - I_{dark}$) dependence of the incident power density is presented in Figure 4b. The photocurrent ($I_{ph}$) exhibits an increased step response when the incident power density increases. Notably, the generated photocurrent is unstable and drifting upward, which may be caused by the self-heating effect as previously reported.[26] The inset shows the response and recovery times at different excited power density. From the statistical data, it is observed that at high power density both of the response and recovery time are 66 ms. The deviation of response time from 66 ms at low power density may be attributed to the slow separation of bound excitons in the junction.[35] The reproducible photoresponse of the p–n diode is also performed as shown in Figure S4 (Supporting Information).

The values of photocurrent in Figure 4b are successively derived and put together with the $I_{ph}$ at the negative bias of −2 V as shown in Figure 4c, elucidating that the photocurrent can be enhanced through increasing the bias voltage. Here, the EQE is introduced to estimate the performance of the p–n photodiode, which is defined as following: EQE = $(I_{ph}/e)/(P_{in}/\hbar v)$, where $P_{in}$, $\hbar$, and $v$ are the incident power, Planck's constant, and speed of light, respectively. According to the stated data at −2 V bias ($V_D$ = −2 V) in Figure 4c, the EQE under different excited power density can be deduced. To explore the influence of the treated $MoS_2$ thickness on the EQE, a heterojunction p–n photodiode with about 42 layers $MoS_2$ was also conducted at the same condition. Figure 4d systematically shows the related EQEs of the two photodiodes with different $MoS_2$ thickness. For both of the photodiodes, the EQE gradually decreases as the power density increases. The photodiode with six layers $MoS_2$ exhibits high EQE than the one with about 42 layers $MoS_2$. Due to the bandgap transition from direct to indirect, $MoS_2$ samples with thin thickness have a high photoelectric conversion efficiency, resulting in the different EQEs between the two devices. Notably, the p–n photodiode with six layers $MoS_2$ has the highest EQE of 52.7% at the drain bias of −2 V. To interpret the selection of wavelength, its photocurrent ($I_{ph}$) versus wavelength is plotted in Figure 4e at the negative bias of −2 V and the power density of 900 mW $cm^{-2}$. Since the direct bandgaps of $MoS_2$ and ZnO are 1.85 eV (680 nm) and 3.4 eV (367 nm), respectively, ultraviolet light could excite both of the two semiconductors while the visible light could only excite $MoS_2$. Therefore, as the wavelength varies from near-ultraviolet (335 nm) to near-infrared (785 nm), the generated photocurrent decreases from 1.4 to 0 µA.

The emerging piezophototronic effect is to use the inner-crystal piezopotential in the piezoelectric semiconductors as a


© 2016 WILEY-VCH Verlag GmbH & Co. KGaA, Weinheim
Adv. Mater. 2016,
DOI: 10.1002/adma.201506472

"gate" voltage to modulate the charges separation, transport, or recombination in optoelectronic devices.[39] This interesting effect could effectively increase the light-emission of LEDs or the photocurrent of photodetectors.[32,40–42] Here, the enhanced photoresponse of the p-type $MoS_2$ and n-type ZnO photodiode by the piezophototronic effect is also investigated. The schematic diagram of the testing set-up is shown in **Figure 5**a. A transparent acrylic plate connected to a digital force gauge is fixed on the junction to conveniently not only apply a uniform pressure, but also transmit the incident ultraviolet. Ineluctably, light scattering effect in the transparent acrylic plate will decrease the incident power illuminating the junction, as indicated in Figure 5b, compared with the $I_{ph}$ in Figure 4c. As the applied pressure increases, the relevant $I_{ph}$ also increases. The inset in Figure 5b depicts the EQE as a function of the applied pressure, indicating that the EQE will be distinctly enhanced for more than four times with the applied pressure increased to 23 MPa.

Figure 5c schematically states the underlying physical mechanism of the observed behaviors with applied pressure. Under the equilibrium state, a barrier at the interface will form due to the different work-function and electron affinity between $MoS_2$ and ZnO.[13] At a reverse bias, the Fermi-levels of those two semiconductors will produce an energy difference, depleting more holes in p-type $MoS_2$ and more electrons in n-type ZnO, which is beneficial to the separation of photogenerated carriers.[35] As previously reported, the odd-layer $MoS_2$ flakes have piezoelectric effect.[8] Since the sample used here is even-layer (six layers), the increased photocurrent (EQE) with external pressure applied is attributed to the piezopotential caused by the ZnO film in the junction area. When the external pressure is applied on the ZnO film, the superposition of electric dipole moment along the *c*-axis in the crystal generates negative and positive piezoelectric charges along the positive and negative *c*-axis, respectively. The ZnO film deposited by PLD in this p–n junction is *c*-axis orientation (Figure 2b) and its positive *c*-axis pointing away from the $MoS_2$ flake (or the substrate). The positive piezoelectric charges yielded at bottom surface of ZnO film will lower the barrier at the interface and make the conductive and valence bands of ZnO film go downward, which is equivalent to enlarging the depletion zone as shown on the right-hand diagrams of Figure 5c. This will contribute to the generation and separation of photogenerated carriers in the p–n heterojunction. Therefore, under an applied pressure, the photocurrent (EQE) can be effectively tuned by the piezophototronic effect.

In summary, we demonstrate a $MoS_2$- and ZnO-based heterojunction p–n photodiode. The as-exfoliated $MoS_2$ flake is doped by the $SF_6$ plasma-assistant method while the ZnO film is deposited by PLD. The p–n diode exhibits sharply gate-tunable electrical characteristics, high rectification ratio ($3.4 \times 10^4$), and large reverse saturation current area (1.5 V). The heterojunction p–n diode presents good photoresponse at the ultraviolet range, the highest EQE of which can reach 52.7% at the reverse bias of –2 V. Additionally, the relevant photocurrent can be distinctly enhanced for more than four times with 23 MPa applied pressure owing to the piezophototronic effect. This work provides a new way to achieve high performance of electronic and optoelectronic devices based on the 2D materials.

## Experimental Section

*Fabrication of the p-Type $MoS_2$ and n-Type ZnO Diode*: During the $SF_6$ plasma treatment, the radio frequency power was fixed at 80 W, the time at 60 s, and the reactive pressure at 2 Pa. At these controllable conditions, the chosen $MoS_2$ samples with thickness about 20–50 nm could be thinned to atomic layer and nearly completely doped. After treating with $SF_6$ plasma, the $MoS_2$ samples were patterned by UV photolithography, on which insulating layers ($Al_2O_3$) of about 30 nm were successively deposited by ALD. Next, the UV photolithography was used again to define the area for synthesizing high-quality ZnO film with a thickness of ≈300 nm, which will be grown by PLD. The laser energy of PLD was set as 300 mJ, the deposited pressure as 5 Pa, the time as 40 min, and the reactive substrate temperature as 200 °C. Finally, Cr/Au (5 nm/50 nm) were deposited on the patterned vertical p–n heterojunctions based on $MoS_2$ and ZnO as the source and drain electrodes by electron beam evaporation. All of the output or transfer curves were measured by the Keithley semiconductor parameter analyzer (4200).

## Supporting Information

Supporting Information is available from the Wiley Online Library or from the author.

## Acknowledgements

This research was supported by the "thousands talents" program for pioneer researcher and his innovation team, China, National Natural Science Foundation of China (Grant Nos. 51432005, 5151101243, and 51561145021).

Received: December 31, 2015
Revised: January 27, 2016
Published online:

[1] B. Radisavljevic, A. Radenovic, J. Brivio, V. Giacometti, A. Kis, *Nat. Nanotechnol.* **2011**, *6*, 147.
[2] S. Kim, A. Konar, W. S. Hwang, J. H. Lee, J. Lee, J. Yang, C. Jung, H. Kim, J. B. Yoo, J. Y. Choi, Y. W. Jin, S. Y. Lee, D. Jena, W. Choi, K. Kim, *Nat. Commun.* **2012**, *3*, 1011.
[3] H. Li, Z. Yin, Q. He, H. Li, X. Huang, G. Lu, D. W. Fam, A. I. Tok, Q. Zhang, H. Zhang, *Small* **2012**, *8*, 63.
[4] Z. Y. Yin, H. Li, H. Li, L. Jiang, Y. M. Shi, Y. H. Sun, G. Lu, Q. Zhang, X. D. Chen, H. Zhang, *ACS Nano* **2012**, *6*, 74.
[5] O. Lopez-Sanchez, D. Lembke, M. Kayci, A. Radenovic, A. Kis, *Nat. Nanotechnol.* **2013**, *8*, 497.
[6] G. Fiori, F. Bonaccorso, G. Iannaccone, T. Palacios, D. Neumaier, A. Seabaugh, S. K. Banerjee, L. Colombo, *Nat. Nanotechnol.* **2014**, *9*, 768
[7] K.-A. N. Duerloo, M. T. Ong, E. J. Reed, *J. Phys. Chem. Lett.* **2012**, *3*, 2871.
[8] W. Z. Wu, L. Wang, Y. Li, F. Zhang, L. Lin, S. M. Niu, D. Chenet, X. Zhang, Y. Hao, T. F. Heinz, J. Hone, Z. L. Wang, *Nature* **2014**, *514*, 470.
[9] H. Zhu, Y. Wang, J. Xiao, M. Liu, S. Xiong, Z. J. Wong, Z. Ye, Y. Ye, X. Yin, X. Zhang, *Nat. Nanotechnol.* **2015**, *10*, 151.
[10] J. Qi, Y. W. Lan, A. Z. Stieg, J. H. Chen, Y. L. Zhong, L. J. Li, C. D. Chen, Y. Zhang, K. L. Wang, *Nat. Commun.* **2015**, *6*, 7430.
[11] K. F. Mak, C. Lee, J. Hone, J. Shan, T. F. Heinz, *Phys. Rev. Lett.* **2010**, *105*, 136805


© 2016 WILEY-VCH Verlag GmbH & Co. KGaA, Weinheim

[12] R. Ganatra, Q. Zhang, *ACS Nano* **2014**, *8*, 4074.
[13] L. B. Chen, F. Xue, X. H. Li, X. Huang, L. F. Wang, J. Z. Kou, Z. L. Wang, *ACS Nano* DOI: 10.1021/acsnano.5b07121.
[14] F. Xue, L. B. Chen, L. F. Wang, Y. K. Pang, J. Chen, C. Zhang, Z. L. Wang, *Adv. Funct. Mater.* DOI:10.1002/adfm.201504485.
[15] B. L. Liu, L. Chen, G. Liu, A. N. Abbas, M. Fathi, C. W. Zhou, *ACS Nano* **2014**, *8*, 5304.
[16] F. K. Perkins, A. L. Friedman, E. Cobas, P. M. Campbell, G. G. Jernigan, B. T. Jonker, *Nano Lett.* **2013**, *13*, 668.
[17] R. Cheng, D. Li, H. Zhou, C. Wang, A. Yin, S. Jiang, Y. Liu, Y. Chen, Y. Huang, X. F. Duan, *Nano Lett.* **2014**, *14*, 5590.
[18] M. Y. Li, Y. M. Shi, C. C. Cheng, L. S. Lu, Y. C. Lin, H. L. Tang, M. L. Tsai, C. W. Chu, K. H. Wei, J. H. He, W. H. Chang, K. Suenaga, L. J. Li, *Science* **2015**, *349*, 524.
[19] K. Roy, M. Padmanabhan, S. Goswami, T. P. Sai, G. Ramalingam, S. Raghavan, A. Ghosh, *Nat. Nanotechnol.* **2013**, *8*, 826.
[20] W. J. Yu, Y. Liu, H. Zhou, A. Yin, Z. Li, Y. Huang, X. Duan, *Nat. Nanotechnol.* **2013**, *8*, 952.
[21] X. P. Hong, J. Kim, S. F. Shi, Y. Zhang, C. H. Jin, Y. H. Sun, S. Tongay, J. Q. Wu, Y. F. Zhang, F. Wang, *Nat. Nanotechnol.* **2014**, *9*, 682.
[22] N. J. Huo, J. Kang, Z. M. Wei, S. S. Li, J. B. Li, S. H. Wei, *Adv. Funct. Mater.* **2014**, *24*, 7025.
[23] J. S. Ross, P. Klement, A. M. Jones, N. J. Ghimire, J. Yan, D. G. Mandrus, T. Taniguchi, K. Watanabe, K. Kitamura, W. Yao, D. H. Cobden, X. Xu, *Nat. Nanotechnol.* **2014**, *9*, 268.
[24] M. R. Laskar, D. N. Nath, L. Ma, E. W. Lee, C. H. Lee, T. Kent, Z. Yang, R. Mishra, M. A. Roldan, J.-C. Idrobo, S. T. Pantelides, S. J. Pennycook, R. C. Myers, Y. Wu, S. Rajan, *Appl. Phys. Lett.* **2014**, *104*, 092104.
[25] M. Chen, H. Nam, S. Wi, L. Ji, X. Ren, L. Bian, S. Lu, X. Liang, *Appl. Phys. Lett.* **2013**, *103*, 142110.
[26] D. H. Li, R. Cheng, H. L. Zhou, C. Wang, A. X. Yin, Y. Chen, N. O. Weiss, Y. Huang, X. F. Duan, *Nat. Commun.* **2015**, *6*, 7509.
[27] Y. Li, C. Y. Xu, J. Y. Wang, L. Zhen, *Sci. Rep.* **2014**, *4*, 7186.
[28] F. Xue, L. M. Zhang, W. Tang, C. Zhang, W. M. Du, Z. L. Wang, *ACS Appl. Mater. Interfaces* **2014**, *6*, 5955.
[29] F. Xue, L. M. Zhang, X. L. Feng, G. F. Hu, F. R. Fan, X. N. Wen, Z. Li, Z. L. Wang, *Nano Res.* **2015**, *8*, 2390.
[30] J. Zhou, Y. D. Gu, P. Fei, W. J. Mai, Y. F. Gao, R. S. Yang, G. Bao, Z. L. Wang, *Nano Lett.* **2008**, *8*, 3035.
[31] W. Z. Wu, X. N. Wen, Z. L. Wang, *Science* **2013**, *340*, 952.
[32] X. Y. Li, M. X. Chen, R. M. Yu, T. P. Zhang, D. S. Song, R. R. Liang, Q. L. Zhang, S. B. Cheng, L. Dong, A. L. Pan, Z. L. Wang, J. Zhu, C. F. Pan, *Adv. Mater.* **2015**, *27*, 4447.
[33] S. M. Niu, Y. F. Hu, X. N. Wen, Y. S. Zhou, F. Zhang, L. Lin, S. H. Wang, Z. L. Wang, *Adv. Mater.* **2013**, *25*, 3701.
[34] X. N. Wen, W. Z. Wu, Y. Ding, Z. L. Wang, *Adv. Mater.* **2013**, *25*, 3371.
[35] S. M. Size, K. K. Ng, *Physics of Semiconductor Devices*, John Wiley & Sons, New York **1981**.
[36] D. Jariwala, V. K. Sangwan, C. C. Wu, P. L. Prabhumirashi, M. L. Geier, T. J. Marks, L. J. Lauhon, M. C. Hersam, *Proc. Natl. Acad. Sci. USA* **2013**, *110*, 18076.
[37] Y. Jin, D. H. Keum, S. J. An, J. Kim, H. S. Lee, Y. H. Lee, *Adv. Mater.* **2015**, *27*, 5534.
[38] H. M. Li, D. Lee, D. Qu, X. Liu, J. Ryu, A. Seabaugh, W. J. Yoo, *Nat. Commun.* **2015**, *6*, 6564.
[39] C. F. Pan, L. Dong, G. Zhu, S. M. Niu, R. M. Yu, Q. Yang, Y. Liu, Z. L. Wang, *Nat. Photonics* **2013**, *7*, 752.
[40] X. Han, W. M. Du, R. M. Yu, C. F. Pan, Z. L. Wang, *Adv. Mater.* **2015**, *27*, 7963.
[41] M.-C. Wong, L. Chen, M.-K. Tsang, Y. Zhang, J. Hao, *Adv. Mater.* **2015**, *27*, 4488.
[42] Y. Zhang, G. Gao, H. L. W. Chan, J. Dai, Y. Wang, J. Hao, *Adv. Mater.* **2012**, *24*, 1729.


© 2016 WILEY-VCH Verlag GmbH & Co. KGaA, Weinheim

DOI: 10.1002/adma.201506472